New methodology for adjusting rotating shadowband irradiometer measurement

Frank Vignola, Josh Peterson, Stefan Wilbert, Philippe Blanc, Norbert Geuder, Christian Kern

New Methodology for Adjusting Rotating Shadowband Irradiometer Measurements

Frank Vignola[1,a)], Josh Peterson[1], Stefan Wilbert[2], Philippe Blanc[3], Norbert Geuder[4], and Chris Kern[5]

[1]*PhD, Department of Physics, University of Oregon, Eugene, Oregon 97403-1274, USA.*
[2]*DLR, Institute of Solar Research, Qualification, 04200 Tabernas, Spain*
[3]*MINES ParisTech, PSL Research University, O.I.E. = Centre Observational, Impact, Energy, France*
[4]*Hochschule für Technik Stuttgart, Stuttgart, Germany*
[5]*Irradiance, USA*

[a)]Corresponding author: fev@uoregon.edu

Abstract. A new method is developed for correcting systematic errors found in rotating shadowband irradiometer measurements. Since the responsivity of photodiode-based pyranometers typically utilized for RSI sensors is dependent upon the wavelength of the incident radiation and the spectral distribution of the incident radiation is different for the Direct Normal Irradiance and the Diffuse Horizontal Irradiance, spectral effects have to be considered. These cause the most problematic errors when applying currently available correction functions to RSI measurements. Hence, direct normal and diffuse contributions are analyzed and modeled separately. An additional advantage of this methodology is that it provides a prescription for how to modify the adjustment algorithms to locations with different atmospheric characteristics from the location where the calibration and adjustment algorithms were developed. A summary of results and areas for future efforts are then discussed.

INTRODUCTION

The rotating shadowband irradiometer (RSI) is frequently deployed to measure global horizontal irradiance (GHI) and diffuse horizontal irradiance (D_fHI) that are used to calculate the direct normal irradiance (DNI). An RSI measures the GHI irradiance and a band rotates approximately once a minute in front of the pyranometer to block direct sunlight and the (D_fHI) is then measured. The Direct Horizontal Irradiance (D_rHI) is then calculated by subtracting the D_fHI irradiance from the GHI irradiance. The DNI is obtained by dividing the calculated D_rHI by the cosine of the solar zenith angle (SZA) (see Eq. 1).

$$DNI = (GHI - D_fHI)/Cos(SZA) \quad (1)$$

Because a fast response time is needed for many of these instruments a photodiode pyranometer is used to record the incident irradiance. As with other pyranometers, these photodiode pyranometers also have characteristics that generate systematic errors. To decrease the uncertainties in measurements generated by RSI instruments, algorithms have been developed that partly correct of these systematic errors. This article reviews the adjustment algorithms made to the RSI measurements and suggests an alternate method of determining the algorithms that may be more relevant for photodiode pyranometers used in RSIs.

Photodiode-based pyranometers utilize solar cells and produce signals that are roughly proportional to incident solar irradiance. However, as with solar cells, a more detailed analysis of photodiode-based pyranometers show that they respond to the number of photons at each wavelength and not the energy contained in each photon. Comparisons

Nomenclature

DNI - Direct Normal Irradiance	RSI - Rotating Shadowband Irradiometer
D_rHI - Direct Horizontal Irradiance	RSP - Rotating Shadowband Pyranometer
GHI - Global Horizontal Irradiance	AHF - Absolute Cavity Radiometer
D_fHI - Diffuse Horizontal Irradiance	CHP1 - Kipp & Zonen pyrheliometer
SZA - Solar Zenith Angle	$R_{LICOR}(\lambda)$ – LI-COR Pyranometer's Spectral Responsivity
T_{amb} - Ambient Temperature	R - Average Responsivity
λ - Wavelength	

with broadband thermopile instruments that respond to the energy of the incident radiation, show that corrections are needed to translate this dependence on the number of photons to the energy contained in the photons. This spectral to broadband adjustment is relatively small for GHI because the spectral distribution of incoming GHI does not change a great deal with changes in atmospheric conditions and solar position partially as a result of the relatively wide spectral response of the silicon solar cell used for the photodiode-based pyranometers. The nature and magnitude of these spectral adjustments are presented in detail in this study.

For many uses of irradiance data, it is the total energy that is important and not the number of photons at each wavelength: incident broadband solar energy is required for modelling solar thermal systems and concentrating solar power plants and the validation of model derived DNI values and the spectral distribution of this energy is relevant to the output of a photovoltaic module or a photodiode-based pyranometer.

Good DNI resource information are required to evaluate perspective locations for concentrating solar thermal electric systems. RSIs are often chosen because of their price and ability to operate remotely with minimal maintenance. Several studies have been published [1 - 14] on methods to correct the spectral dependence of RSI instruments to obtain more accurate GHI, D_fHI, and DNI measurements.

The best GHI values are obtained by projecting the DNI from an absolute cavity radiometer onto a horizontal surface and adding a diffuse irradiance obtained from pyranometer with minimal thermal offset and a good cosine and spectral response. Comparison of the photodiode pyranometer and the reference GHI values identified several systematic errors with these instruments. Correction algorithms were developed to account for these systematic errors [1, 2, 5 - 9]. These procedures worked well for the global horizontal irradiance (GHI) and include functions that correct the effects of temperature, spectral dependence, and cosine response of these photodiode pyranometers.

While these correction algorithms are very useful, questions remain about the applicability of these correction algorithms to locations with disparate climate conditions.

Later studies [3, 13] showed that photodiode-based pyranometers systematically underestimate the diffuse irradiance under clear skies by 20 to 30%. Under clear sky conditions, Rayleigh scattering is the dominant source for the diffuse irradiance. Since Rayleigh scattering is highly wavelength dependent (λ^{-4}), the diffuse irradiance has a larger contribution of photons in the blue region of the spectrum as compared to the distribution of sunlight coming directly from the sun. The different between the spectral distribution of the D_fHI irradiance under clear skies and the DNI spectral irradiance is the reason that photodiode pyranometers underestimate the D_fHI under clear skies conditions.

Since the D_fHI contribution is only around 10 to 20 % of GHI on under clear skies, the error associated with the underestimate of the D_fHI results in an increase estimate of the instrument's GHI responsivity. Under cloudy conditions, the D_fHI and GHI are the same and therefore the photodiode-based pyranometers provided fairly reliable measures of the GHI. To provide a more accurate description of the pyranometer's behavior, two calibrations constants are really required, one for the D_rHI and one for the D_fHI component.

These spectral effects begin to assume an importance when photodiode-based pyranometers were incorporated into Rotating Shadowband Irradiometers (RSI). The problems caused by the reduced responsivity to diffuse irradiance were soon discovered and the correction models [1, 2, and 3] were used to adjust the RSI measurements. Significant improvements in the accuracy of RSI reading were made. For a detailed discussion of RSIs, see [4].

Current methodologies to obtain the adjustment algorithms that are used to account for the systematic errors associated with photodiode pyranometers utilized by RSIs include:

- Corrections to the global and diffuse measurements to account for the temperature dependence of the pyranometer
- Prescription to account for the spectral dependence with change in air mass of the photodiode pyranometer on GHI measurements
- Formulas to correct the cosine response associated with the lens optics
- Adjustments to the D_fHI measurements to account for the different spectral distribution of D_fHI as opposed to the spectral distribution of the GHI.

The improvement obtained by using these corrections is significant and tests were conducted to validate the improvements [1-3, 9-14].

Other methods [8, 12] have been discussed about calibrating a photodiode-based pyranometer besides the standard pyranometer calibration method of comparing against a reference standard pyranometer.

Many of these instruments are deployed in areas with atmospheric conditions that deviate greatly from areas where the instruments were developed and tested. Since the algorithms were mainly developed and tested in the mid-northern hemisphere it may be advantageous to modify the adjustment algorithms for areas that have significantly different atmospheric conditions [16]. This is specifically true for spectral adjustments that depend on the spectral distribution of the incident irradiance.

The article is organized as follows. The new methodology is described and then it is implemented with data from Eugene, Oregon. A comparison between the standard methodology and the new methodology is then conducted. This is followed by a discussion of how to apply this methodology to other areas along with possible future directions. Studies from areas with somewhat differing atmospheric conditions ranging from areas with a dry and moderate climate to areas with high temperatures and considerable aerosol loaded atmospheric conditions have been analyzed and presented in [10] and [11] with generally good correlation.

NEW METHODOLOGY FOR CORRECTION RSI SYSTEMATIC ERRORS

Because the RSI instruments provide both the DNI and D_fHI values, it becomes possible to evaluate and calibrate the DNI and the D_fHI components separately. While the temperature effect on responsivity vary with wavelength and the spectral distribution of DNI and D_fHI are significantly different under clear sky conditions [4, 13, 16], it is assumed, for this investigation, that the components have the same temperature correction. With an understanding of how the D_rHI and the D_fHI components are affected by changing spectral distributions, it is possible to determine the average spectral response of each component and use this information for the calibration of the RSI instrument and determine the other adjustments that need to be made to account for other uncertainties [15, 16].

It is useful to make the temperature adjustments before evaluating and incorporating the other adjustments because the temperature adjustments are assumed to be identical for both the D_rHI and D_fHI components. The validity of this assumption is a topic for future research.

The next step in this alternate approach is to use the RSI to provide the D_rHI and D_fHI components from the photodiode-based pyranometer and calibrate each component against reference DNI and D_fHI measurements. By evaluating each component separately, a more direct approach is provided for ascertaining the uncertainty in each component and this can lead to independent testing of the adjustment algorithms. This is different from calibrating the pyranometer's GHI (or DNI) measurements against reference GHI (or DNI) values and deriving one calibration constant for the instrument. The average GHI spectral responsivity is really a combination of the average DNI and D_fHI spectral responsivities under clear skies and this proportion of the D_rHI and D_fHI contributions to the GHI value vary over the day. As has been shown in [16], the changing proportions of D_rHI and D_fHI components to the GHI value and their respective changes in their responsivity over the day somewhat offset each other and yield GHI responsivity that is relatively constant over the day when compared to the changes in the DNI and D_fHI responsivities.

While this method is well defined under clear skies, the D_fHI spectral distribution is different under cloudy or partially cloudy conditions. It has been found that under cloudy conditions, the D_rHI responsivity is very similar to the D_rHI responsivity under clear skies [16]. In contrast to that, the D_fHI responsivity under cloudy conditions changes and approaches the D_rHI responsivity. It has been suggested by Michalsky in [4] that clouds act as neutral density filters and pass the irradiance through without significantly altering the spectral distribution. Under clear skies, the D_fHI contribution is small and the D_rHI average spectral responsivity dominates the GHI responsivity. Under cloudy skies the D_fHI average spectral responsivity is similar to the D_rHI's. Therefore the calibrations found for GHI measurements under clear skies, where the spectral D_rHI responsivity dominates, works well under clear and cloudy conditions.

The deviation from true cosine response of the pyranometer requires another adjustment factor [1-2]. Most of this correction is related to the diffusor disk of the LI-COR pyranometer. This adjustment is determined after the spectral adjustment has been made. The D_fHI is much less sensitive to the deviation from true cosine response because DfHI comes from all parts of the sky. It is assumed that the effect of the deviation from true cosine response for D_fHI measurements averages to a constant that would be incorporated into the calibration. Future studies would be needed to determine the validity of this assumption.

MODELING THE DNI COMPONENT

To demonstrate the new methodology, irradiance data from Eugene, Oregon, USA and Payerne, Switzerland were utilized. An Ascension Rotating Shadowband Pyranometer (RSP) without any adjustments is operated alongside instruments at the solar test facility in Eugene. During this period, a calibration using an absolute cavity radiometer (Eppley AHF) was used for the reference DNI measurements and the reference D_fHI comes from a shadowball shaded Schenk Star pyranometer.

The spectral distribution of DNI is somewhat dependent on atmospheric water vapor and aerosols, it is largely independent of cloud cover because clouds cause DNI to scatter and become D_fHI and minimally change the spectral distribution of DNI. This is illustrated in Fig. 1 where the average DNI spectral responsivity falls in a narrow band that is mainly a function of solar zenith angle. The data is from all weather conditions where the sum of the spectral DNI from 320 to 1030 nm is greater than 10 W/m^2. The spectral range used, 320 to 1030nm, is that of the PMOD spectral radiometer used to obtain the DNI spectral data. Discussion of the selected wavelength range and data used to generate this plot can be found in reference [16].

The new methodology is based upon the characterization of the spectral response of the photodiode-based pyranometer and the systematic change in spectral distribution of incident irradiance over the day. The average responsivity of the photodiode-based pyranometer to the spectral distribution of the incident radiation is dependent upon the spectral response of the pyranometer $R_{LICOR}(\lambda)$ as shown in Eqn. 2 where λ is the wavelength. The DNI and D_fHI spectral distributions are different and in this methodology, the DNI and D_fHI spectral adjustment factors are studied separately making it easier to examine the effects of spectral distribution on each component without being significantly influenced by the other component. This method results in two calibration constants one for the DNI and another for the D_fHI.

$$R = \frac{\sum_{300}^{4000} R_{LICOR}(\lambda) * DNI(\lambda)}{\sum_{300}^{4000} DNI(\lambda)} \tag{2}$$

To get an idea of the sensitivity of the responsivity of a photodiode-based pyranometer to the instrument's spectral responsivity, two spectral responsivities were examined. The theoretical LI-COR spectral responsivity was available from the manufacturer. The National Renewable Energy Laboratory (NREL) has measured the spectral responsivity of several LI-COR pyranometers and one measurement of the spectral responsivity was chosen to compare against the data from LI-COR - see Fig. 2. The consequence of selecting a specific LI_COR spectral responsivity is illustrated in Fig. 3 where the results from the two spectral distributions in Fig. 2 are used. The measured spectral responsivity shows an enhancement on the blue end of the spectral and the near infrared end of the spectrum as compared to the

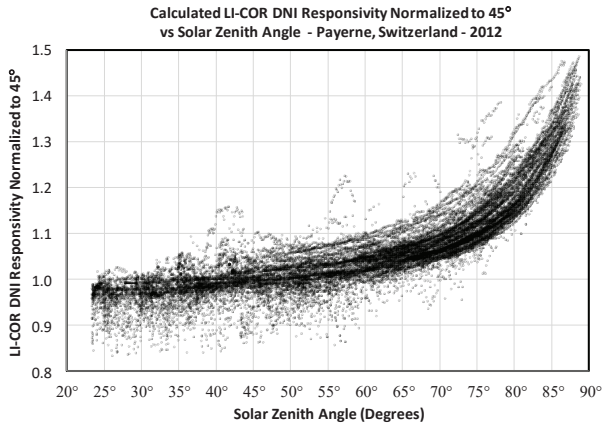

FIGURE 1. Plot of calculated DNI responsivity as a function of solar zenith angle for DNI>10W/m^2. Generic LI-COR spectral responsivity combined with spectral DNI data.

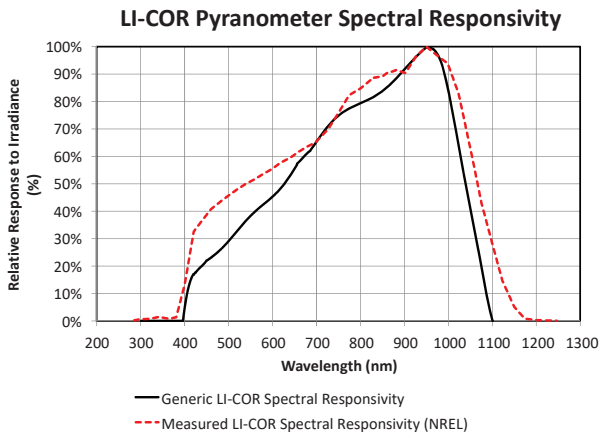

FIGURE 2. Plot of generic and measured LI-COR spectral responsivities.

generic estimate of the spectral responsivity. The area under the two curves is different and this difference is taken into account when the convoluted data are normalized.

The average DNI responsivity was calculated using Equation 2 with a wavelength range from 300 to 1200 nm and the spectral data came from a LI-1800 spectroradiometer. Since the LI-1800 only measures irradiance in the 300 to 1100 nm range, the SMARTS2 model [17] was used to extend the range to 1200 nm to cover the wavelengths where the pyranometer responds. The modeled average DNI responsivity was then compared to measured DNI irradiance over the day.

The average DNI responsivity was calculated using Eqn.2 with a modified wavelength range of 300 to1200 nm (instead of 300 to 4000 nm) and the spectral data came from a LI-1800 spectroradiometer. Since the LI-1800 only measures irradiance in the 300 to 1100 nm range, the SMARTS2 model [17] was used to extend the range to 1200 nm to cover the wavelengths where the pyranometer responds. The modeled average DNI responsivity was then compared to measured DNI irradiance over the day.

To determine the average DNI responsivity, a calibration was performed on July 10, 2014 using the Eppley AHF cavity radiometer for the reference 1-min DNI values and a shaded Schenk Star pyranometer for the reference D_fHI values. The DNI value from the RSI was obtained from the uncorrected D_fHI and GHI using Eqn. 1 and accurate SZA calculations [4]. The temperature dependence of the pyranometer was then taken into account by multiplying the data values by

$$(1.-0.00082*(T_{amb}-25)) \tag{3}$$

where T_{amb} is the ambient temperature in Celsius. The parameters for this formula were determined in a study by King et. al. [1] where "T" is interpreted as ambient temperature.

The next step in the calibration procedure was to adjust the responsivity of the RSI pyranometer so that the ratio of the RSI DNI values divided by the reference DNI value from the cavity radiometer was equal to 1 when the SZA was equal to 45°. The 45° angle was chosen as it is often used when calibrating pyranometers. Figure 3 is a plot of the three modeled and one measured set of DNI values divided by the reference DNI values from the cavity radiometer. The curves on the plot are modeled estimates of the spectral effect using Equation 2 using a 300 to 1200 nm range. The formula for the models were taken from half hourly DNI spectral values calculated for Eugene in July 15, 2013 using the SMARTS2 model. Both the theoretical and measured LI-COR spectral responsivities were convoluted with the spectral data and the resulting average responsivities determined. Again these responsivities and the King air mass function [1] were normalized to 1 at a SZA of 45°. The King air mass adjustment function matches the data fairly well and is the basis for RSI adjustment factors. The theoretical LI-COR spectral responsivity was not a very good fit to the data so only the measured LI-COR spectral responsivity and the King model will be used in the rest of the discussions.

The measured and modeled LI-COR spectral responsivity as shown in Fig. 2 don't seem that much different, but the average spectral responsivity determined for each can be significantly different. Therefore, having good spectral

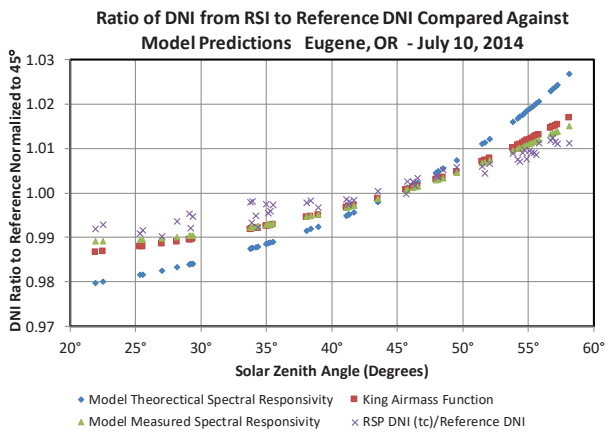

FIGURE 3. Ratio of DNI estimate or measure divided by the reference DNI normalized to 1.00 at 45º. The King air mass correction function is shown here for comparison.

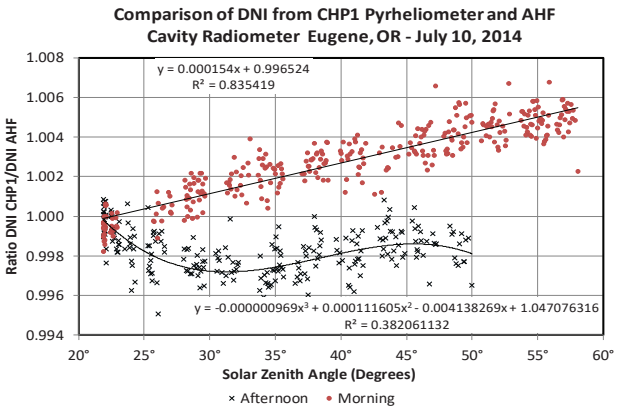

FIGURE 4. Ratio of DNI values from the CHP1 pyrheliometer and the AHF cavity radiometer under clear skies.

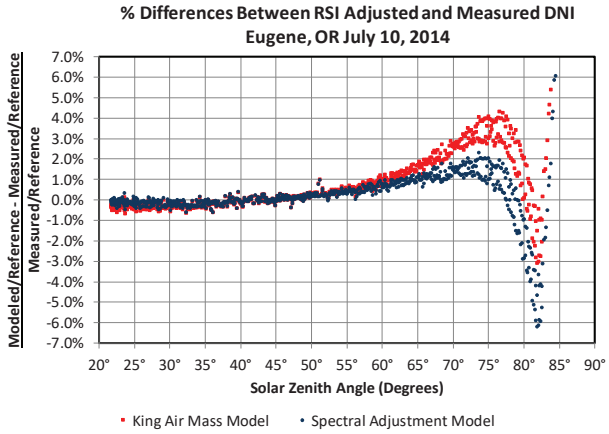

FIGURE 5. Relative difference between the ratio of modeled and measured DNI divided by the reference DNI data from a CHP 1 pyrheliometer plotted against SZA.

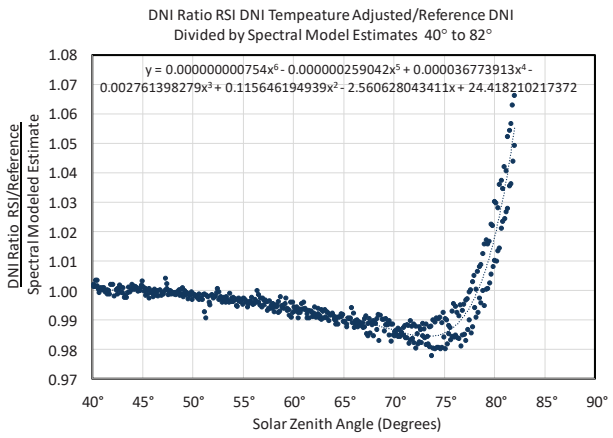

FIGURE 6. Angle of incident adjustment factor for the RSI DNI component for SZA between 40º and 82º after the spectral adjustment is made.

response information on the pyranometer can be important and a good match between the data and model is important. It also shows that a good calibration can be obtained if an appropriate spectral responsivity for the instrument has been chosen.

It should be noted that there is only a ±1% difference between the RSI DNI values and the reference DNI values over the 20° to 60º range and much of this difference is mimicked by the models. Therefore, it is of interest to look at what happens at large SZA when the change in spectral distribution is expected to have a larger effect. While the main interest of the original study was to determine a calibration constant for the RSI instrument, other instruments were run and calibrated on July 10, 2014. One such instrument was a Kipp & Zonen CHP1 pyrheliometer. While the deviation of the ratio from the reference DNI values is small, the calibration information for the CHP1 pyrheliometer was used to adjust the CHP1 DNI values during the whole day (see Fig. 4).

Using the adjusted CHP1 data as reference DNI data, the RSI DNI values can be studied over the whole day and not just when there was cavity data (see Fig. 5). From 20° to 55° the agreement between the corrected CHP1 values and the adjusted RSI DNI values is better than 0.5%, about the same range of agreement between the unadjusted CHP1 values and the AHF Cavity DNI values. From 55° to about 80° the spectral correction model still produces results that are within ±2% of the adjusted CHP1 values. As with most pyranometers at larger SZA, the deviation from true cosine response starts to affect the readings.

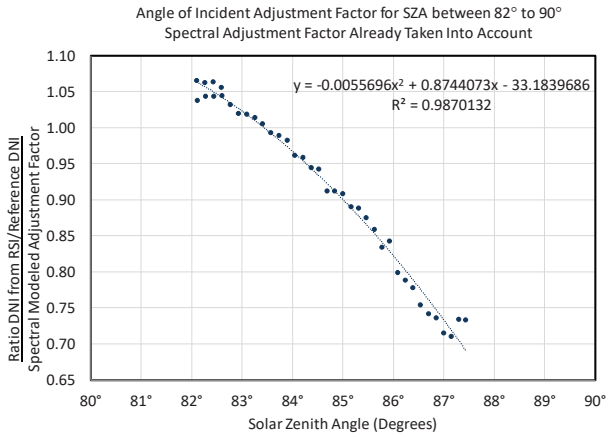

FIGURE 7. Angle of incident adjustment factor for the RSI DNI component for SZA between 82º and 90º after the spectral adjustment is made.

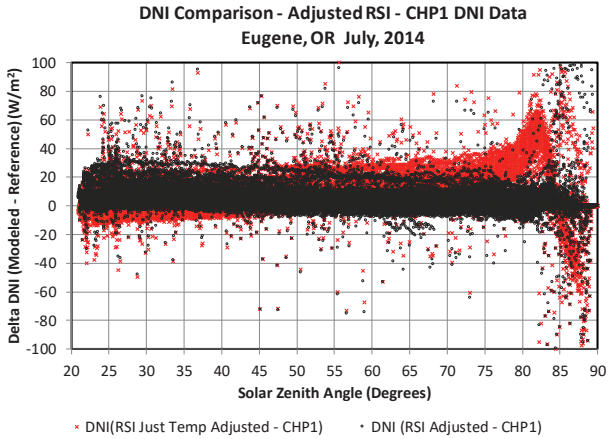

FIGURE 8. Comparison of adjusted RSI DNI values (black dots) minus the CHP1 DNI measurements and unadjusted RSI DNI values (red dots) for July, 2014 in Eugene, Oregon.

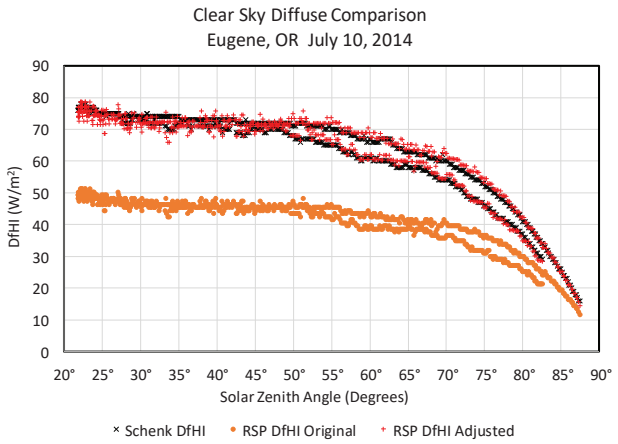

FIGURE 9. Clear sky D_fHI values from reference pyranometer, RSI unadjusted, and RSI adjusted data.

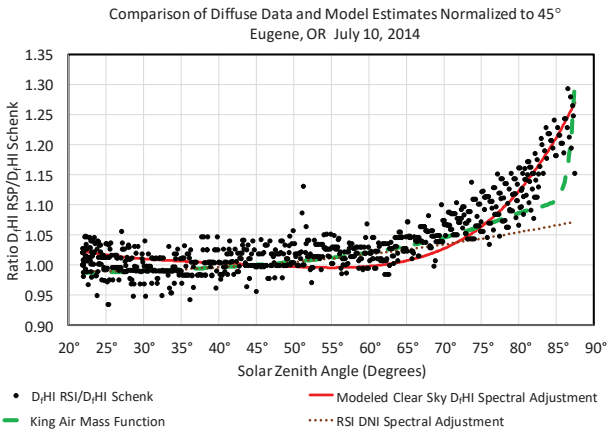

FIGURE 10. Comparison of D_fHI values from reference measurements and modeled estimated.

Therefore, an algorithm was devised to adjust the RSI readings to match the corrected CHP1 DNI values. This will be called the cosine adjustment factor. This DNI cosine adjustment factor is theoretically independent from the spectral response correction, but any error in the spectral adjustment could be incorporated into the factor accounting for the deviation from true cosine response. This factor is developed for the RSI DNI values in this method and not for the GHI values as is done with some models [6, 9, 12]. It is assumed that this cosine adjustment factor will differ slightly between LI-COR pyranometers and this is an initial attempt to characterize this adjustment factor. There is a sharp change at 82°, so the cosine adjustment factor will be divided into two parts, from 50° to 82° and 82° to 90° (See Figures 6 and 7).

To test the model DNI algorithms under all weather conditions, adjustments were made to all RSI DNI 1-min values generated in July 2014 and compared with 1-min average DNI values from the CHP 1 pyrheliometer. The comparison is shown in Fig. 8. The average is about 5 W/m^2 higher and the standard deviation is 21 W/m^2. There was smoke intrusion from a forest fire that affected the last day in July. As shown, this did result in a significant difference between the DNI from the adjusted RSI data and the broadband pyrheliometer. This results in the band of data points that run 20 to 30 W/m^2 above the CHP 1 values in Fig. 8.

DETERMINATION OF THE AVERAGE D_fHI SPECTRAL RESPONSIVITY UNDER CLEAR SKIES

The formula for D_fHI spectral adjustment was obtained in a similar manner to that for the DNI spectral adjustment factor. The SMARTS2 model was used to obtain the spectral distribution of incident diffuse irradiance on July 15, 2013. The measured LI-COR spectral responsivity was convolved with the D_fHI spectral data as in Eqn. 2 with the DNI spectral distribution replaced with the D_fHI spectral distribution. The result yielded the clear sky diffuse spectral adjustment factor. Because water vapor and aerosols can significantly affect the D_fHI, the diffuse spectral adjustment factor is an approximation whose accuracy can vary with atmospheric conditions.

A comparison of the D_fHI from the RSI to the reference Schenk D_fHI measurement is shown in Fig. 9 under clear skies. The D_fHI calibration is determined after adjusting for temperature and multiplying by the equation for the D_fHI the clear sky spectral adjustment. Then the calibration is determined by matching the D_fHI from the RSI with the reference D_fHI at a SZA of 45°. A perusal of Fig. 9 show that the adjusted RSI D_fHI values fairly well match the reference D_fHI values under clear sky conditions. The change necessary to increase the RSI D_fHI value as the sun gets lower in the sky (larger solar zenith angle) decreases. This change in adjustment factor is also shown in Fig. 10 which plots the ratio of the original D_fHI from the RSI to the D_fHI from the Schenk. This figure shows that just normalizing the RSI D_fHI values at 45° brings the unadjusted clear sky D_fHI values to within ±5% of the reference for D_fHI values for solar zenith angles less than 60°. When the clear sky RSI D_fHI values are adjusted to reflect the change in the spectral distribution of the irradiance, the resulting D_fHI have a standard deviation of ±5% with respect to the reference diffuse values. This is an equivalent to a 95% uncertainty of approximately ±3.5 W/m^2.

MODELING THE D_FHI RESPONSIVITY UNDER CLOUDY SKIES

Under totally overcast skies, the GHI and the D_fHI values are the same and the LI-COR pyranometer's GHI values are similar to that of reference GHI values. Under clear skies, the D_rHI component dominates and one can assume that the incident global spectral distribution seen are very similar to the spectral distribution of the D_rHI component plus a small contribution from the D_fHI irradiance. If one assumes that clouds act as a neutral density filter, then the spectral distribution seen by the RSI sensor is basically the D_rHI spectral distribution. Intermediate states where the sky is only partially covered by clouds then the diffuse spectral radiation must be some combination of D_rHI and the D_fHI spectral contributions.

The ratio of one-minute D_fHI data from the RSI and the Schenk pyranometer are shown in Fig. 11 for July 2014 in Eugene, Oregon. Periods of clear sky populate the bottom band and totally overcast skies populate the top band. The spectral effect modeled using the clear sky spectral values from the SMARTS2 model and convoluted with the measured LI-COR spectral responsivity is shown as the line that goes through the clear sky values. Two tasks must be accomplished to model the D_fHI component adjustments under all sky conditions. First the clear sky periods must be separated from the cloudy periods. This was done in the following manner.

- If SZA < 65° and DNI RSI Adjusted > 600 W/m^2 and D_fHI < 60 W/m^2, then clear sky conditions were assumed.
- If 65° < SZA < 80° and DNI RSI Adjusted > 200 W/m^2 and D_fHI < 60 W/m^2 then clear sky conditions were assumed.
- If 80° < SZA < 90° and D_fHI RSI Adjusted < 60 W/m^2 then clear sky conditions were assumed
- Else cloudy conditions were assumed.

After removing the clear sky periods from the data set, a correlation between the ratio of the RSI D_fHI values and the Schenk D_fHI values was run to determine the adjustment function for the RSI D_fHI adjustment.

$$\text{RSI } D_fHI/\text{reference } D_fHI = \text{Clear Sky } D_fHI \text{ adjustment} * F(D_fHI) + [1 - F(D_fHI)]*\text{DNI RSI Adjustment.} \quad (4)$$

This is a result of combing the DNI spectral adjustment during cloudy periods with the D_fHI adjustment factor for clear periods. The polynomial to the sixth degree with zero intercept $F(D_fHI)$ (see Table 1) is used to determine the proportion of clear and cloudy skies.

For consistency, the D_fHI values were adjusted for the temperature dependence before the values were used for the ratio and the correlation. In order to prevent spurious adjustment values for data at the upper end, it was estimated that with the percentage function $F(D_fHI)$ was set equal to 0.05 when D_fHI was greater than 400 W/m^2.

The resulting percent difference between the adjusted RSI D_fHI values and the reference D_fHI values is shown in Fig. 12. The average difference between the RSI adjusted D_fHI and the reference D_fHI is 0.1 W/m^2 and the standard error is ±7.8 W/m^2.

TABLE 1. Diffuse partition function, $F(D_fHI)$, parameters

	a	b	c	D	e	f
Coefficients	2.659189E-02	-3.626073E-04	1.969852E-06	-5.205345E-09	6.651340E-12	-3.287586E-15
Standard error (%)	0.9%	1.4%	1.9%	2.4%	2.8%	3.3%

$$F(D_fHI)= a*D_fHI+b*D_fHI^2+c*D_fHI^3+d*D_fHI^4+e*D_fHI^5+f*D_fHI^6$$

RESULTS AND DISCUSSION

Using the new methodology, a RSI was calibrated and adjustment algorithms were developed. Comparison between the reference measurements and the adjusted RSI components are shown in Figs. 8 and 12. These results compare well with measured data and current algorithms developed for RSIs. The air mass adjustment factors of previous models have been replaced by spectral adjustment factors.

The following steps are a summary of used to obtain the adjustments for the RSI.

1. Obtain spectral responsivity of the pyranometer used in the RSI
2. Using a spectral irradiance model, calculate the DNI spectral irradiance distribution at different times of the day under clear sky conditions.
3. Calibrate the DNI component of the RSI against a reference DNI measurements.

4. Normalize the measured DNI responsivity at various solar zenith angles to the average responsivity measured at 45°.
5. Estimate the spectral effect at various SZAs on the average DNI responsivity by multiplying the pyranometer spectral responsivity by the modeled incident spectral DNI and divide by the average DNI irradiance determined from the spectral model. Normalize to 45°.
6. Compare the measured spectral responsivity against the modeled spectral responsivity. Determine the difference between to measured and modeled values and assume this difference is caused by the deviation from the true cosine response.
7. Using a spectral irradiance model, calculate the DfHI spectral irradiance distribution at different times of the day under clear sky conditions.
8. Calibrate the DfHI component of the RSI against a reference DfHI measurement under clear sky conditions.
9. Normalize the measured DfHI responsivity at various solar zenith angles to the average responsivity measured at 45°.
10. Determine the average DfHI responsivity during cloudy periods as a function of DrHI responsivity and DfHI responsivity.
11. Using the 45º average responsivity. Apply adjustments determined from the model as a function of SZA to the RSI measurements.
12. It is posited that one can obtain RSI adjustments for a new location by using the ratio of responsivity calculated with a spectral irradiance model along with the instrument spectral responsivity for the location of interest divided by similarly obtained values for the location where the instrument was calibrated.

The advantage of this methodology is that spectral models, such as SMARTS2 [17], can be used to modify the spectral affects associated with the atmospheric conditions where the instrument was calibrated and adjusted to specific local atmospheric conditions. The new adjustment factors are obtained by modifying the adjustment factors by the ratio of the adjustment factors calculated with the atmospheric inputs to the SMARTS2 model for new location by the similar adjustment factor calculated using atmospheric inputs for the location of the original calibrations. This has to be done for both the DNI and D_fHI adjustment factors. This alteration can be notably important if atmospheric aerosol composition at the new location is significantly different from the locations where the instrument was calibrated.

The results presented here assumed that the spectral dependence of the LI-COR photodiode-based pyranometer was the same as the spectral dependence measured for a different instrument at NREL. Comparing the spectral predictions using a generic spectral dependence and the measured spectral dependence shows that the results are fairly sensitive to the spectral dependence used for the pyranometer. It is very difficult to separate the deviation from true cosine response of the pyranometer from the spectral response of the pyranometer because they both vary with the solar zenith angle. To separate the cosine from the spectral response, one would have to change the angle of incidence while maintaining the spectral distribution of the irradiance. This could be done by tilting the RSI with respect to the incident DNI and evaluating how the resulting tilted diffuse component changes.

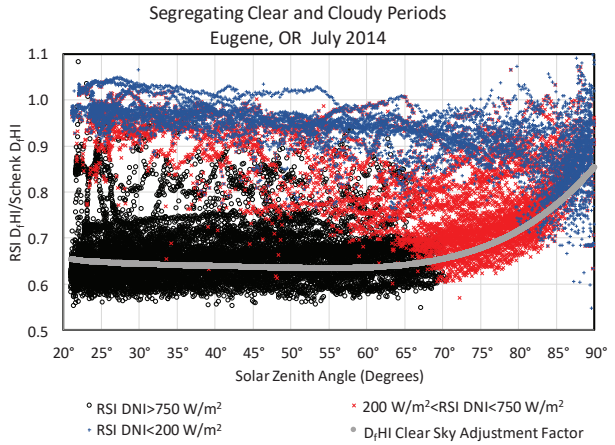

FIGURE 11. Segregating the ratio of reference and temperature adjusted RSI measured D_fHI into different sky conditions.

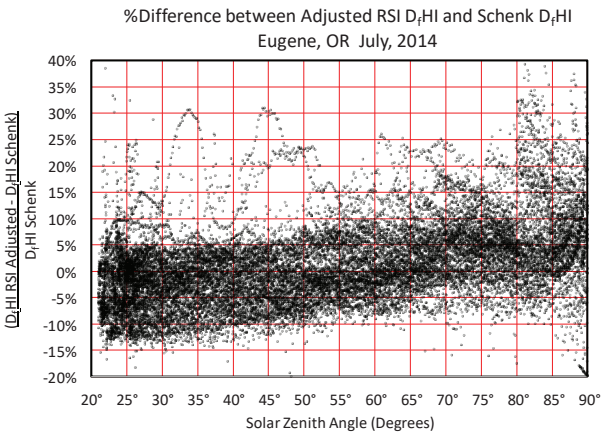

FIGURE 12. Percent difference between adjusted RSI and reference D_fHI for July, 2014 in Eugene, Oregon

While the clear sky DNI spectral adjustment factor can be applied under all weather conditions, this is not true for the clear sky D_fHI spectral adjustment factor. A formula was found that enabled the D_fHI spectral adjustment factor to be determined for all weather conditions using a combination of the clear sky DNI spectral adjustment factor and the clear sky D_fHI spectral adjustment factor. Therefore, the D_fHI spectral adjustment factor can also be modified to local atmospheric conditions.

This was an initial attempt test the feasibility of this methodology and it is expected that refinements can be made to this methodology. Areas for future research are:

- Evaluation of the methodology against RSI measurements made over a much longer time span.
- Obtaining a more comprehensive set of pyranometer spectral responsivities to test the sensitivity of the methodology to changes in the spectral responsivity
- Characterizing and modeling of the effects of water vapor on the calculated spectral adjustments.
- Modeling the spectral responsivity in areas with completely different spectral distribution characteristics to determine the uncertainties associated with characterizing specific locations and what can be done to modify the algorithms to these other locations.
- Examination of the methodology with different instruments and locations to determine common characteristics and identify characteristics that are site or season specific.

Now that this new methodology has been demonstrated to work for photodiodes pyranometers, future efforts will examine if a similar spectral adjustment methodology would be applicable to performance models for photovoltaic modules.

ACKNOWLEDGEMENTS

We would like to thank the Bonneville Power Administration, the Energy Trust of Oregon, and the National Renewable Energy Laboratory under subcontract XAT-6-62159-01 for support of the University of Oregon Solar Radiation Monitoring Laboratory that made this part of this work possible. Funding for other contributions from the EU FP7 project SFERA2 for DLR's contribution is appreciated. We would also like to thank NREL for the measured spectral responsivity data of a LI-COR pyranometer.

REFERENCES

1. D. King and D. Myers, "Silicon-Photodiode Pyranometers: Operational Characteristics, Historical experiences, and New Calibration Procedures," 26th IEEE Photovoltaic Specialists Conference, Sept. 29-Oct. 3, 1997, Anaheim, California, 1997.
2. D. King, J. A. Dratochvil, and W. E. Boyson, "Measuring Solar Spectral and Angle–of–Incidence Effects of Photovoltaic Modules and Solar Irradiance Sensors", 26th IEEE Photovoltaic Specialists Conference, Sept. 29-Oct. 3, 1997, Anaheim, California, 1997.
3. F. Vignola, Solar Cell Based Pyranometers: Evaluation of Diffuse Responsivity, *Proceedings of the 1999 Annual Conference American Solar Energy Society*, 260, June 1999.
4. F. Vignola, J. Michalsky, and T. Stoffel. 2012. Solar and Infrared Radiation Measurements. CRC Press
5. J. Augustyn, T. Geer, T. Stoffel, R. Kessler, E. Kern, R. Little, and F. Vignola. 2002. Improving the accuracy of low cost measurement of direct normal irradiance. Proceedings of the American Solar Energy Society, R. Campbell-Howe and B. Wilkins-Crowder (eds.), American Solar Energy Society, Boulder, Colorado, USA.
6. Augustyn, J., T. Geer, T. Stoffel, R. Kessler, E. Kern, R. Little, F. Vignola, and B. Boyson. 2004. Update of algorithm to correct direct normal Irradiance measurements made with a rotating shadow band pyranometer. Proceedings of the American Solar Energy Society, R. Campbell-Howe and B. Wilkins-Crowder (eds.), American Solar Energy Society, Boulder, Colorado, USA.
7. Vignola, F. 2006. Removing systematic errors from rotating shadowband pyranometer data. In Proceedings of the American Solar Energy Society, R. Campbell-Howe, ed., American Solar Energy Society, Boulder, CO.
8. Geuder, N., N, Pulvermueller, B, Vorbrugg, O., 2008. Corrections for rotating shadowband pyranometers for solar resource assessment, Proceedings of SPIE 70460, International Society for Optical Engineering, Society of Photo-Optical Instrumentation Engineers.

9. Geuder, N., Hanussek, M., Haller, J., Affoler, R., Wilbert, S. 2011. Comparison of Corrections and Calibration Procedures for Rotating Shadowband Irradiance Sensors. SolarPACES Conference, Granada, Spain.
10. Geuder, N., Affolter, R., Goebel, O., Dahleh, B., Al Khawaja, M., Wilbert, S., Pape, B., and Pulvermueller, B., 2016. "Validation of Direct Beam Irradiance Measurements from Rotating Shadowband Irradiometers (RSI) in a Region with Different Atmospheric Conditions." Journal of Solar Energy Engineering. doi: 10.1115/1.4034070.
11. Geuder, N., Affoler, R., Kraas, B., Wilbert, S., 2014. Long-term behavior, accuracy and drift of LI-200 pyranometers as radiation sensors in Rotating Shadowband Irradiometers (RSI). Energy Procedia 49 (2014), 2330-2339.
12. Jessen, W., S. Wilbert, et al. (2016). "Calibration methods for rotating shadowband irradiometers and optimizing the calibration duration." Atmos. Meas. Tech. 9(4): 1601-1612.
13. Wilbert, S., S. Kleindiek, et al. (2016). "Uncertainty of rotating shadowband irradiometers and Si-pyranometers including the spectral irradiance error." AIP Conference Proceedings 1734(1): 150009.
14. Myers, DR. 2011. Quantitative analysis of spectral impacts on silicon photodiode radiometers. Paper read at Solar Conf., Raleigh, NC, (17–21 May 2011).
15. The Payerne instrument performance evaluation is a contribution to the project Direct Normal Irradiance Nowcasting methods for optimized operation of concentrating solar technologies (DNICast). DNICast received funding from the European Union's Seventh Programme for research, technological development and demonstration under grant agreement No 608623.
16. F. Vignola, Z. Derocher, J. Peterson, L. Vuilleumier, C. Félix, J. Gröbner, N. Kouremeti, 2016. Effects of changing spectral radiation distribution on the performance of photodiode pyranometers, Solar Energy 129, (2016) 224-235.
17. Gueymard, Christian, A., 2006. SMARTS code, version 2.9.5 for Windows—User's Manual.